A highly optimized quantum algorithm for accurate simulations of two-site dynamical mean-field theory on noisy quantum hardware

Thomas Steckmann
Department of Physics, North Carolina State University, Raleigh, North Carolina 27695, USA

Yan Wang
Quantum Computational Science Group, Oak Ridge National Laboratory, Oak Ridge, Tennessee 37831, USA

(Dated: August 2021; Revised 13 August 2021)

Dynamical mean-field theory (DMFT) maps the solution of the Hubbard model for strongly correlated electronic systems to solution of the Anderson impurity model consisting of a quantum impurity coupled to a noninteracting bath system, where electrons only interact when they doubly occupy the impurity site. Quantum algorithms have been proposed to speed up solving the impurity model by preparing and evolving the ground state under the impurity Hamiltonian, which is the most expensive part of the calculation for DMFT. To improve existing algorithms for the two-site DMFT problem and overcome the difficulty of simulating on noisy quantum hardware, we propose a highly optimized quantum circuit, which (i) prepares the ground state with only three controlled-NOT (CNOT) gates and a single variational parameter and (ii) evolves the state over any time with a fixed depth quantum circuit based on Cartan decomposition that has no Trotter error. For simulating long time evolution on noisy quantum hardware, our Cartan based method results in shorter circuit and is thus more accurate than the method based on Trotter decomposition.

I. INTRODUCTION

The physical properties of quantum systems consisting of many interacting particles, such as the transition temperature of a superconductor, can be difficult to compute or predict accurately using classical computers. To encode and process information about a quantum system, classical computers require storage and or runtime that increases exponentially with the number of particles in the system. As a result, digital quantum computers are poised to become better tools to tackle these challenging physical problems: they avoid the exponential scaling problem by storing and processing information using quantum bits (qubits) that are precisely controlled and programmed quantum systems. Ultimately, quantum computers with many error-corrected logic qubits will be available, but in the near term state-of-the-art quantum systems are limited in applications to quantum computing due to the presence of quantum noise.

Implementing algorithms on so called noisy intermediate-scale quantum (NISQ) computers to perform even simple computations remains challenging by short coherence times and noisy gate operations. In prior computation work studying the dynamics of interacting electrons, it was observed that even over very small time scales, Trotter based approaches to approximate time evolution lead to nonphysical results: comparing to theoretical values, simulations on the quantum computer give inaccurate frequencies of the time evolution for the two-site Anderson impurity model system, which are symptoms of decoherence or approximation errors.[1] For NISQ systems, the Trotter approximation leads to the dilemma: it becomes exact in the limit of an infinite-depth circuit, so more accurate simulations require increased gate counts, but increasing gate count reduces simulation fidelity due to accumulated noise.

In this work, we approach the problem of NISQ simulations by demonstrating an application of Cartan decomposition to two-site dynamical mean-field theory (DMFT) on state-of-the-art quantum hardware. Cartan decomposition allows for exact fast-forwarding of Hamiltonian simulation by applying a time-independent unitary rotation to the Hamiltonian in a Lie algebraic representation to produce a Hamiltonian that has only commuting terms (elements in the Cartan subalgebra) and thus is easy to exponentiate with an exponent linearly proportional to time of the evolution. Once the unitary rotation is obtained, the exponent parameters of the commuting terms can be trivially updated in the quantum circuits to simulate the Hamiltonian at any time for the same gate cost.[2] For many-body systems such as the Anderson impurity model (AIM) used in DMFT, the computation cost of the exact Cartan decomposition increases exponentially with increasing number of bath energy levels (i.e., bath sites). However, for small number of bath sites, it remains manageable and allows us to explore whether this method is capable to extract physically accurate results from noisy hardware, where Trotter based methods fail. Additionally, the structure of Cartan decomposition allows for more simplifications which result in a highly optimized circuit that can be tailored to execute on specific hardware architectures. With such Cartan based quantum circuit, we are able to extract accurate low frequency signals from simulations of the two-site DMFT on NISQ systems.

II. MODEL HAMILTONIANS

A. The Hubbard model

The Hubbard model Hamiltonian is given by

$$\hat{H}_{\text{Hubbard}} = -\tilde{t} \sum_{\langle i,j\rangle,\sigma} (\hat{c}^\dagger_{i\sigma}\hat{c}_{j\sigma} + \hat{c}^\dagger_{j\sigma}\hat{c}_{i\sigma}) + U\sum_i \hat{n}_{i\uparrow}\hat{n}_{i\downarrow} - \mu\sum_{i,\sigma}\hat{n}_{i,\sigma}, \tag{1}$$

where $\hat{c}^\dagger_{i\sigma}$ ($\hat{c}_{i\sigma}$) is the electron creation (annihilation) operator for electron with spin $\sigma \in \{\uparrow,\downarrow\}$ at lattice site i; $\hat{n}_{i\sigma} = \hat{c}^\dagger_{i\sigma}\hat{c}_{i\sigma}$ is the electron density operator; $\tilde{t}$ is the hopping integral ("tunneling") which we typically choose as units of energy by setting $\tilde{t} = 1$; U is the Coulomb interaction; and μ is the chemical potential. Here, $\langle i,j\rangle$ refers to indices of nearest-neighbor sites on the lattice.[3]

B. Anderson impurity model and dynamical mean-field theory

Exact simulations of the Hubbard model in the general case are limited to dozens or hundreds of particles, far from the large number of particles which would be considered in the macroscopic (thermodynamic) limit. Dynamical mean-field theory is a significant development in studying the Hubbard model for such large systems.[4] In the limit of a lattice with infinite dimensions (∞-d), such as ∞-d hypercubic lattice and Bethe lattice, meaning each lattice site is directly connected to infinitely many other lattice sites, DMFT exactly maps the solution of the Hubbard model to that of the Anderson impurity model (AIM), where the temporal correlations are accurately captured. The interacting electrons in the Hubbard model in the thermodynamic limit (i.e., *infinite* lattice sites) is reduced to electrons interacting on a single quantum impurity site coupled to a bath of *continuous* single-particle energy levels that electrons can hop onto. In numerical simulations, we describe the energy levels as discrete bath lattice sites denoted by ϵ_i with index $i \in \{1,\ldots,N_b\}$. We denote the on-site energy of the impurity ϵ_0. For nonmagnetic states we consider, these parameters do not depend on the electron spin quantum number. The final Anderson impurity model Hamiltonian is given by

$$\hat{H}_{\text{AIM}} = \sum_{i=1,\sigma}^{N_b} V_i(\hat{c}^\dagger_{0,\sigma}\hat{c}_{i,\sigma} + \hat{c}^\dagger_{i,\sigma}\hat{c}_{0,\sigma}) + U\hat{n}_{0,\uparrow}\hat{n}_{0,\downarrow} + \sum_{i=0,\sigma}^{N_b}(\epsilon_i - \mu)\hat{n}_{i,\sigma}, \tag{2}$$

where V_i is the coupling (tunneling) between the impurity site (site index 0) and bath sites (site index $\{1,\ldots,N_b\}$). The Coulomb interaction term (second term in the above Hamiltonian) only involves the impurity site. In numerical simulation, the infinite levels of the bath must be approximated using as many levels as can be computed. The simplest of these approximations is two-site DMFT, which includes a single bath site ($N_b = 1$) and a single impurity site.

III. QUANTUM ALGORITHM FOR TWO-SITE DMFT

A. Jordan-Wigner transformation of Hamiltonian to Pauli (qubit) operators

Fermionic Hamiltonians cannot be implemented directly onto a quantum computer. First, we must employ a mapping from the fermionic operator algebra to the qubit operator algebra composed of Pauli strings: permutations of the Pauli matrices at each qubit site combined via the Kronecker tensor product. The Jordan-Wigner transformation[5] is one of such methods that we will use. We denote Pauli matrices as $X = \left(\begin{smallmatrix}0&1\\1&0\end{smallmatrix}\right)$, $Y = \left(\begin{smallmatrix}0&-i\\i&0\end{smallmatrix}\right)$, and $Z = \left(\begin{smallmatrix}1&0\\0&-1\end{smallmatrix}\right)$ and the identity matrix $I = \left(\begin{smallmatrix}1&0\\0&1\end{smallmatrix}\right)$. The Pauli strings for N-qubit system are the Kronecker tensor products of N Pauli or identity matrices. We define $Z_i = I^{\otimes(i-1)} \otimes Z \otimes I^{\otimes(N-i)}$ for the type of Pauli strings acting on only a single qubit. The standard procedure follows an algorithm to map the fermionic basis states to the computational basis spanned by a sequence of qubits and the fermionic operators to the sum of Pauli string operators on these qubits. This is given as follows.

1. Map fermionic states to qubit states. We employ a mapping where the spin-orbitals $|i\sigma\rangle$ for the same spin but different sites are grouped together $|0\uparrow, 1\uparrow, \cdots, 0\downarrow, 1\downarrow, \cdots\rangle$. Occupied states are $|1\rangle$ in the computational basis, and unoccupied states are $|0\rangle$.

2. Apply $\hat{c} \to \hat{\sigma}_+ = \frac{1}{2}(X + iY)$ and $\hat{c}^\dagger \to \hat{\sigma}_- = \frac{1}{2}(X - iY)$. From these two identities, we also get $\hat{n} \to \frac{1}{2}(I - Z)$ and $\hat{h} \to \frac{1}{2}(I + Z)$.

3. To maintain canonical anticommutation relations for fermion operators $\left\{\hat{c}_{j\sigma}, \hat{c}^\dagger_{j'\sigma'}\right\} = \delta_{jj'}\delta_{\sigma\sigma'}$ and $\left\{\hat{c}_{j\sigma}, \hat{c}_{j'\sigma'}\right\} = \left\{\hat{c}^\dagger_{j\sigma}, \hat{c}^\dagger_{j'\sigma'}\right\} = 0$, map the indexed fermionic operators (site index $0 \le j \le N_b$) to the corresponding qubit operators as follows.

$$\begin{aligned}
\hat{c}_{j\uparrow} &= \frac{1}{2} Z_1 \cdots Z_{j-1}(X_j + iY_j), & \hat{c}^\dagger_{j\uparrow} &= \frac{1}{2} Z_1 \cdots Z_{j-1}(X_j - iY_j), \\
\hat{c}_{j\downarrow} &= \frac{1}{2} Z_1 \cdots Z_{N_b+j}(X_{N_b+1+j} + iY_{N_b+1+j}), & \hat{c}^\dagger_{j\downarrow} &= \frac{1}{2} Z_1 \cdots Z_{N_b+j}(X_{N_b+1+j} - iY_{N_b+1+j}), \\
\hat{n}_{0\uparrow} &= \frac{1}{2}(I_0 - Z_0), & \hat{n}_{0\downarrow} &= \frac{1}{2}(I_{N_b+1} - Z_{N_b+1}).
\end{aligned}$$

In the above, $Z_j \cdots Z_{j'} = \prod_{k=j}^{j'} Z_k$ for $j' \ge j$ and $Z_j \cdots Z_{j'} = 1$ for $j' < j$.

Applying the above steps to the AIM Hamiltonian yields

$$\begin{aligned}
\hat{H}_{\mathrm{AIM}} = &\sum_{i=1}^{N_b} \frac{V_i}{2} \big(X_0 Z_1 \cdots Z_{i-1} X_i + Y_0 Z_1 \cdots Z_{i-1} Y_i \\
&+ X_{N_b+1} Z_{N_b+2} \cdots Z_{N_b+i} X_{N_b+1+i} + Y_{N_b+1} Z_{N_b+2} \cdots Z_{N_b+i} Y_{N_b+1+i} \big) \\
&+ \frac{U}{4}(Z_0 Z_{N_b+1} - Z_0 - Z_{N_b+1}) + \sum_{i=0}^{N_b} \frac{\epsilon_i - \mu}{2}(Z_i + Z_{N_b+1+i}).
\end{aligned} \tag{3}$$

We have dropped a constant term $\frac{U}{4} I_0 I_{N_b+1} = \frac{U}{4}$ from the above Hamiltonian since a constant energy shift does not affect the dynamics of a system.

The Hamiltonian simplifies in the two-site case (one impurity site and $N_b = 1$ bath site). Further, due to particle-hole symmetry of a half-filling (total two particles) ground state we will consider, additional constraints on ϵ_0 and ϵ_1 are as follows: the impurity on-site energy $\epsilon_0 = 0$, so $\epsilon_0 - \mu = -\mu = -\frac{U}{2}$; ϵ_1 must satisfy a self-consistency condition in which the occupation of the impurity site is defined by to the occupation of the Hubbard lattice, which results in $\epsilon_1 - \mu = 0$.[6,7] Therefor, the simplified two-site $\hat{H}_{\mathrm{AIM}}$ with a half-filling ground state is given by

$$\hat{H}_{\mathrm{AIM}} = \frac{V}{2}(X_0 X_1 + Y_0 Y_1 + X_2 X_3 + Y_2 Y_3) + \frac{U}{4} Z_0 Z_2. \tag{4}$$

B. Algorithm for computing Green's function

In DMFT, the dynamics and response of the interacting electron system can be described by the *retarded impurity Green's function* denoted as $G^R_{\mathrm{imp}}(t)$ in the time domain. Specifically, the Green's function describes the propagation of a perturbed system in space and time. In our case, which is Green's function at zero temperature, we consider injecting (removing) a particle from the ground state of the system and, after the perturbation is removed by removing (injecting) a particle, measuring the overlap of the ground state and the final state over time. The impurity Green's function refers to injecting or removing the particles at the impurity site. In this case, there are two possibilities, injecting or removing a spin-↑ particle or a spin-↓ particle, corresponding to the spin-↑ and spin-↓ impurity Green's functions, respectively. But half-filling ground state has zero total spin and is spin-rotationally invariant, spin-↑ and spin-↓ perturbations behave identically. This is known as spin-rotational symmetry. Therefore, we give the impurity Green's function without spin label in terms of fermion operators that has an unspecified spin index σ as follows.

$$G^{\mathrm{R}}_{\mathrm{imp}}(t, t') = -i\theta(t - t') \left\langle \psi_{\mathrm{GS}} \right| \left\{ \hat{c}_{0,\sigma}(t), \hat{c}^\dagger_{0,\sigma}(t') \right\} \left| \psi_{\mathrm{GS}} \right\rangle \tag{5}$$

In the Heisenberg picture, operators $\hat{c}(t)$ are time evolved as $\hat{c}(t) = U^\dagger(t)\hat{c}U(t) = e^{it\hat{H}}\hat{c}e^{-it\hat{H}}$. To simplify the computation, we set $t' = 0$. In the Appendix, we elaborate on the full expansion and subsequent simplification of Green's function after the Jordan-Wigner transform is applied, which results in the relatively inexpensive summation

over only the real components of

$$iG^{\mathrm{R}}_{\mathrm{imp}}(t>0) = \frac{1}{2}\,\mathrm{Re}\,\langle\psi_{\mathrm{GS}}|\,U^{\dagger}(t)X_0U(t)X_0\,|\psi_{\mathrm{GS}}\rangle + \frac{1}{2}\,\mathrm{Re}\,\langle\psi_{\mathrm{GS}}|\,U^{\dagger}(t)Y_0U(t)Y_0\,|\psi_{\mathrm{GS}}\rangle \tag{6}$$

Each term in the summation can be evaluated as the expectation of a single Hadamard-test type quantum circuit using only one time evolution operator in the circuit.

1. *Iteration loop for DMFT*

The DMFT loop refers to the need to update the parameters V_i and ϵ_i in the Anderson impurity model depending on the conditions (such as U and μ) of the Hubbard model being simulated until the system reaches self-consistency. Before the start of the loop, we choose an initial guess for each V_i and ϵ_i. For each iteration of the loop, V_i and ϵ_i computed at end of the previous iteration are used to recompute these the parameters by DMFT self-consistent equations. The iteration loop continues until the recomputed values are sufficiently close to the input V_i and ϵ_i. The specific details are given below.

1. Choose initial values for parameters V_i and ϵ_i. In the two-site model, we fix ϵ_i to specific values to simplify the Hamiltonian. Due to our half-filling constraint, $\epsilon_0 = 0$ and $\epsilon_1 = \frac{U}{2}$ are fixed in the two-site DMFT loop.

2. Evaluate $G^R_{\mathrm{imp}}(t)$ over a selection of time t values. Then, we apply a Fourier transform to this data, so the sampling rate must be above the Nyquist criterion and increasing the time domain of the samples increases the spectral resolution of the transformed Green's function.

3. Find the least-squares fit of the quantum simulated $G^R_{\mathrm{imp}}(t)$ data with the following function form

$$G^R_{\mathrm{imp}}(t>0) = 2[\alpha_1\cos(\omega_1 t) + \alpha_2\cos(\omega_2 t)], \tag{7}$$

   where $\alpha_{1,2}$ and $\omega_{1,2}$ are fitting parameters. Due to the limitations extracting a high resolution Fourier transform of $G^R_{\mathrm{imp}}(t)$ without an inordinate number of samples in time, we fit $G^R_{\mathrm{imp}}(t)$ against a function which is known to encompass the solutions, given half filling and zero net spin.

   Using this analytic form[6,8] as a solution without knowing the exact values of the parameters ($\alpha_{1,2}$ and $\omega_{1,2}$), we can smooth out the influences of noise in the simulation. Additionally, it allows for transforming $G^R_{\mathrm{imp}}(t)$ to $G^R_{\mathrm{imp}}(\omega)$ in frequency domain by exact Fourier integral transform rather than approximating it by discrete Fourier transform.

4. Compute the self-energy $\Sigma_{\mathrm{imp}}(\omega)$ using $G^R_{\mathrm{imp}}(\omega)$ from the previous step. We have the general result[7]

$$G^R_{\mathrm{imp}}(\omega) = \frac{1}{\omega + i\delta - (\epsilon_0 - \mu) - \Delta(\omega) - \Sigma_{\mathrm{imp}}(\omega)}. \tag{8}$$

   We have introduced an artificial broadening term $i\delta$ with $\delta = 0.1$. $\Delta(\omega)$ is the mean-field-like frequency-dependent parameter

$$\Delta(\omega) = \frac{V^2}{\omega - (\epsilon_1 - \mu)}. \tag{9}$$

   Dyson's equation $G^R_{\mathrm{imp}}(\omega) = G^{R(0)}_{\mathrm{imp}}(\omega) + G^{R(0)}_{\mathrm{imp}}(\omega)\Sigma_{\mathrm{imp}}(\omega)G^R_{\mathrm{imp}}(\omega)$, along with the result in Eq. (8) allows us to solve for the self-energy

$$\Sigma_{\mathrm{imp}}(\omega) = \frac{1}{G^{R(0)}_{\mathrm{imp}}(\omega)} - \frac{1}{G^R_{\mathrm{imp}}(\omega)}, \tag{10}$$

   Here, $G^{(0)}_{\mathrm{imp}}(\omega)$ is the non-interacting Green's function with $U = 0$. In the frequency domain, this is exactly

$$G^{R(0)}_{\mathrm{imp}}(\omega) = \frac{1}{\omega - \left(\epsilon_0^{(0)} - \mu^{(0)}\right) - \Delta(\omega)} = \frac{1}{\omega - \Delta(\omega)}. \tag{11}$$

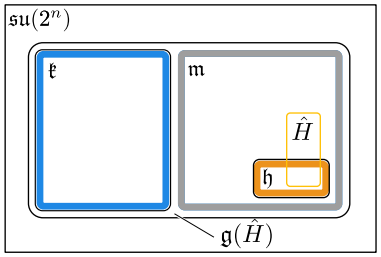

$$\hat{H}_{\mathrm{AIM}} = \frac{V_i}{2}(X_0X_1 + Y_0Y_1 + X_2X_3 + Y_2Y_3) + \frac{U}{4}(Z_0Z_2)$$

$$\mathfrak{g}(\hat{H}) = \left\{ \begin{array}{cccc} X_0Y_1Z_2, & Y_0X_1Z_2, & Z_0X_2Y_3, & Z_0Y_2X_3, \\ Z_1X_2Y_3, & Z_1Y_2X_3, & X_0Y_1Z_3, & Y_0X_1Z_3, \\ Y_0Y_1, & X_0X_1, & Y_2Y_3, & X_2X_3, \\ Z_0Z_1Y_2Y_3, & Z_0Z_1X_2X_3, & Y_0Y_1Z_2Z_3, & X_0X_1Z_2Z_3, \\ Z_0Z_2, & Z_1Z_2, & X_0Y_1X_2Y_3, & X_0Y_1Y_2X_3, \\ Y_0X_1X_2Y_3, & Y_0X_1Y_2X_3, & Z_0Z_3, & Z_1Z_3 \end{array} \right\}$$

FIG. 1. Cartan Decomposition applied to the simplified, two-site Anderson impurity model Hamiltonian.

5. From the self-energy, we compute the quasi-particle weight $\mathcal{Z}$ and update $V_{\mathrm{new}} = \sqrt{\mathcal{Z}}$. There are two approaches to computing this value, using the definition Eq. (12) or the approximation Eq. (13) which integrates over low frequency peaks $\pm\omega_1$ in the spectral function $A(\omega) = -\frac{1}{\pi}\,\mathrm{Im}[G^R_{\mathrm{imp}}(\omega)]$.

$$\mathcal{Z}^{-1} = 1 - \left.\frac{\mathrm{dRe}[\Sigma_{\mathrm{imp}}(\omega)]}{\mathrm{d}\omega}\right|_{\omega=0} \tag{12}$$

$$\mathcal{Z} = \int_{|\omega\pm\omega_1|<4\delta} A(\omega)\,\mathrm{d}\omega \tag{13}$$

Keen *et al.*[1] claimed that the spectral function integral is a better approach due to noisy results, but we determined that the difficulty in computing $\mathcal{Z}$ using Eq. (12) instead arises from the numerical instability of taking the derivative of the self-energy computed using $G^R_{\mathrm{imp}}(\omega)$ fitted to Eq. (7) without exact solutions for the parameters. Instead of computing the derivative in Eq. (12) numerically, we solve the derivative analytically by using the exact Fourier integral transform of Eq. (7), remove the unphysical simple pole of self-energy by assuming a condition obeyed by the exact solution $\frac{2\alpha_1}{\omega_1^2} + \frac{2\alpha_2}{\omega_2^2} = \frac{1}{V^2}$, and finally find Eq. (14), which is equivalent to Eq. (15) that depends only on the parameters ω_1 and ω_2. Eq. (16) is also equivalent and seems to give the best result for the iterations with small V values. In converting Eq. (14) to Eq. (15) and Eq. (16), we again used the condition $\frac{2\alpha_1}{\omega_1^2} + \frac{2\alpha_2}{\omega_2^2} = \frac{1}{V^2}$, as well as the spectral function sum rule $2\alpha_1 + 2\alpha_2 = 1$.

$$\mathcal{Z} = \frac{2(\alpha_1\omega_2^2 + \alpha_2\omega_1^2)^2}{\alpha_1\omega_2^4 + \alpha_2\omega_1^4}, \tag{14}$$

$$\mathcal{Z} = \frac{\omega_1^2\omega_2^2}{V^2(\omega_1^2 + \omega_2^2 - V^2)}, \tag{15}$$

$$\mathcal{Z} = \frac{\alpha_1/\alpha_2}{\alpha_1/\alpha_2 + (1 - V^2/\omega_2^2)^2}. \tag{16}$$

2. *Cartan decomposition*

Our primary contribution is simplifying the time evolution unitary operation $\exp\left(-it\hat{H}_{\mathrm{AIM}}\right)$ in Green's function measurement circuit by applying Cartan decomposition. The standard method based on Trotterization (we also use for comparison) is an approximation of the time evolution circuit which converges in the limit of an infinite depth circuit. Though there are different methods of approaching a Trotter time evolution, we compare our results to the first order Trotter expansion

$$e^{-it\hat{H}} = \left(e^{-i\frac{t}{N}\hat{H}}\right)^N \approx \left(\prod_{l=1}^{M} e^{-i\frac{t}{N}\hat{H}_l}\right)^N \tag{17}$$

where $\hat{H} = \sum_{l=1}^{M}\hat{H}_l$.

For Cartan decomposition, we apply the algorithm described by Kökcü *et al.*[2] and Earp and Pachos[9] to exactly fast-forward the computation of Green's function using a fixed depth quantum circuit. Here, we briefly summarize the algorithm applied to $\hat{H}_{\mathrm{AIM}}$ given in Eq. (4) and also illustrate the steps in Fig. 1. The algorithm is implemented

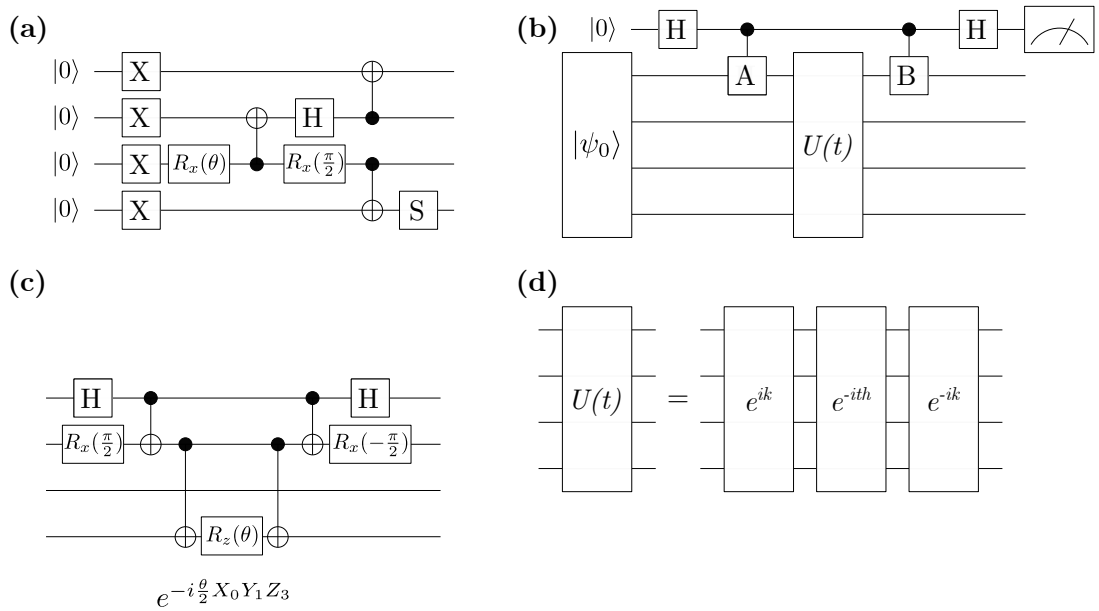

FIG. 2. (a) Ground state ansatz circuit. (b) Interference circuit for measuring the real component of Green's function $\mathrm{Re}\,\langle B(t)A\rangle$. (c) Example Pauli exponential used for time evolution. (d) Block circuit diagram from the decomposition of the time evolution circuit.

in our Cartan Quantum Synthesizer Python package.[10]

1. Generate the *Hamiltonian algebra* $\mathfrak{g}(\hat{H})$ as a subset of the elements of $\mathfrak{su}(2^n)$ through nested commutators with the Hamiltonian.

2. Apply a Cartan involution that places the elements of $\mathfrak{g}(\hat{H})$ with an even count of Y Pauli operator terms in the set $\mathfrak{m}$ and elements with an odd count of Y terms in the subalgebra $\mathfrak{k}$. This results in a Cartan decomposition, which obeys

$$[\mathfrak{m},\mathfrak{m}]\subseteq\mathfrak{k}, \qquad [\mathfrak{k},\mathfrak{k}]\subseteq\mathfrak{k}, \qquad [\mathfrak{m},\mathfrak{k}]\subseteq\mathfrak{m}.$$

3. From $\mathfrak{m}$ find a maximal commuting set $\mathfrak{h}$, which is called a *Cartan subalgebra*.

4. Find a local extremum over the algebra $\mathfrak{k}$ of $f(K)=\langle e^{ik}(v)e^{-ik},\hat{H}\rangle$. Here, $\langle a,b\rangle$ is the Killing form equal to $2\times 2^n\,\mathrm{Tr}(ab)$ on n qubits, and v defined in this work as $v=\sum_i \gamma^i h_i$ where the h_i elements form a basis for $\mathfrak{h}$ and γ is a transcendental number such as π.

5. Compute the vector $h=e^{-ik}(\hat{H})e^{ik}$

The result of the algorithm is a vector $h\in\mathfrak{h}$ and $k\in\mathfrak{k}$ which satisfies $e^{-it\hat{H}}=e^{ik}e^{-ith}e^{-ik}$. Often, additional decomposition is required for e^{ik}, but in the case of two-site DMFT the elements of k commute. Because h is also composed of commuting elements, the full exponential is relatively simple to implement exactly on a quantum computer.

We note that the dimensionality of the Hamiltonian algebra generated by the $\hat{H}_{\mathrm{AIM}}$ scales exponentially with the number of bath sites. However, for the two-site model, the size of the algebra remains manageable. It is of continuing interest to determine if the dimensionality of the Hamiltonian algebra can be constrained to polynomial in the number of bath sites by adopting some effective approximate algorithm.

IV. CIRCUIT IMPLEMENTATION OF THE TWO-SITE DMFT LOOP

Ground State: Two-site DMFT is well studied, and as such we implement a single parameter ground-state ansatz circuit which prepares the ground state for all possible values of V and U. The ansatz in Fig. 2(a) requires only 3 nearest-neighbor CNOTs, and is the simplest known circuit to prepare the needed states. Locating the parameter θ is performed using a simulated Variational Quantum Eigensolver.

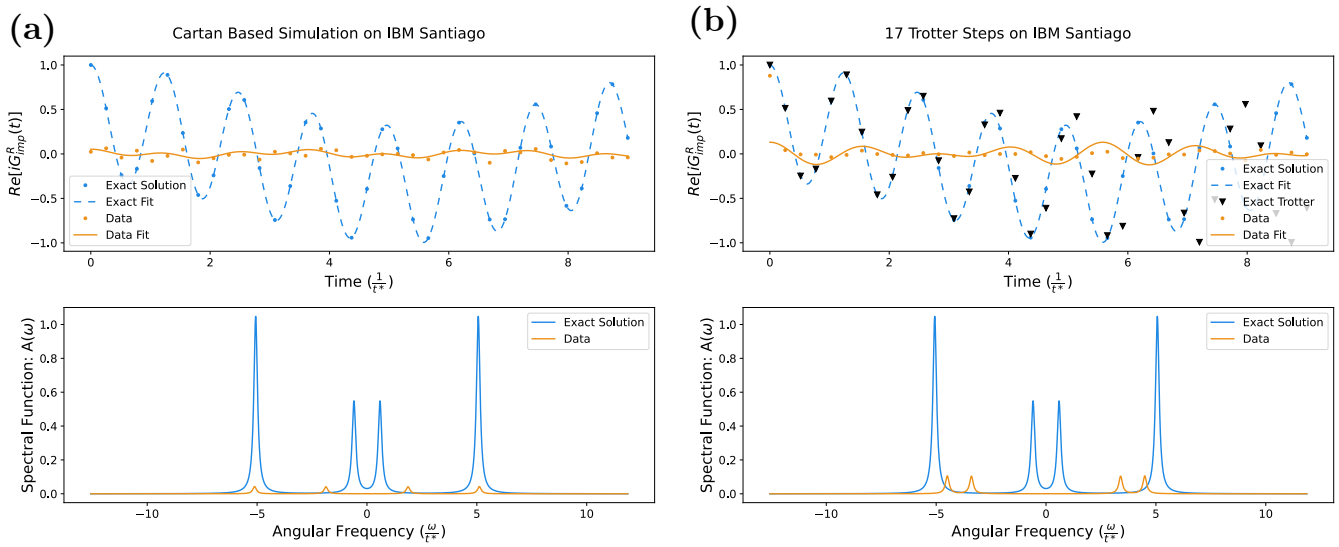

FIG. 3. Green's function evaluations and the spectral function fit on quantum hardware with $V = 1t^*$ and $U = 8t^*$, from which we expect the solution $\alpha_1 = 0.17$, $\alpha_2 = 0.33$, $\omega_1 = 0.59$, and $\omega_2 = 5.06$. Blue points represent data from an exact solution, while orange points are results from IBMQ_Santiago with 8000 shots. The results are post-processed by removing nonphysical results and fitting Eq. (7). (a) Relatively low amplitude results which are fit with $\alpha_1 = 0.013$, $\alpha_2 = 0.013$, $\omega_1 = 1.9$, and $\omega_2 = 5.1$. (b) Result from implementation of the Trotter based circuit, where the black data points represent error from the Trotter approximation. The results are fit with $\alpha_1 = 0.032$, $\alpha_2 = 0.033$, $\omega_1 = 3.39$, and $\omega_2 = 4.49$.

Green's Function: To compute the two terms in Green's function Eq. (6), we use the circuit in Fig. 2(b).[1,7] The circuit introduces an ancilla and adds only 2 CNOT gates to the simulation. The expectation $\mathrm{Re}[\langle \hat{B}(t)\hat{A}\rangle]$ is computed as the expectation of the measurement on the ancilla $\langle Z_a\rangle = \Pr(0_a) - \Pr(1_a)$. Measuring the imaginary component, which is unnecessary in our particular application, can be accomplished by measuring $\langle Y_a\rangle$, requiring only an $R_x(\pi/2)$ gate after the final Hadamard gate.

Time Evolution: Once the specific parameters in the Cartan decomposition are computed via minimization for a given value of V and U, Green's function can be computed at any time with independent, arbitrarily low error. The circuit, along with an example Pauli exponential, is shown in Fig. 2(c)–(d). The circuit requires the exact implementation of, in order, e^{-ik}, e^{-ith}, and e^{-ik}, each of which, before additional simplifications and assuming an all-to-all qubit connectivity, requires 32 CNOT gates. Thus, the total cost of ground state preparation circuit, Green's function interference circuit, and the time evolution circuit is $3 + 2 + 32 \times 3 = 101$ CNOT gates.

Post Processing: Due to the structure of the interference circuit, the measurements of the system qubits are not directly used in computing $\langle Z_a\rangle$, which is only calculated from measured counts of ancilla qubit. However, because of the nature of unitary time evolution and Green's function, the final quantum state of the system qubits must preserve both total spin and total particle number under ideal simulations. Thus, we eliminate measured counts of ancilla qubit whenever the simultaneously measured outcomes of the system qubits indicating the final quantum state violates either of these conditions.

V. RESULTS

Although additional work is required to fully implement the circuit on quantum hardware with minimal gate costs, we have explored the results from initial circuits using using quantum simulations and IBM's quantum hardware. These initial results indicate two key results: (i) Trotterized circuits with the same depth begin to deviate from the expected frequencies in the time domain used for the simulation; (ii) the results of the Cartan based Green's function simulation on physical hardware have low amplitude signals but better maintain information about frequencies.

Fig. 3(a) shows results from the Cartan based simulation using, due to variations in the Qiskit transpiler, an average of 131 CNOTs over a range of 105 to 180 CNOTs on IBM quantum computer Santiago using Qiskit.[11] Each circuit is run over 8000 shots, and spin- or particle-conservation violations account for approximately 6000 shots being dropped from the results, leaving each data point as the expectation of approximately 2000 shots each on two circuits (one circuit for $\mathrm{Re}\,\langle X(t)X\rangle$ and the other $\mathrm{Re}\,\langle Y(t)Y\rangle$). The increase in CNOT count over the all-to-all case of 101 CNOTs

is primarily attributed to need for SWAP gates in non-nearest neighbor Pauli exponentials on the actual quantum computer with only nearest-neighbor qubit connectivity. The background noise results in a very low amplitude signal, though it remains possible to extract reasonably accurate frequencies. ω_2 is in excellent agreement with the expected values, and we expect that increasing the simulation time would provide more accurate results for ω_1.

Even in the absence of hardware noise, Trotter error accumulates over longer time scales since the decomposition error is inherent in the algorithm. For low frequency signals, we expect Trotter based simulation to perform more poorly than Cartan based simulation. In Fig. 3(b), we present the results of a 17 Trotter step simulation of the IBM device Santiago. Transpiling the circuit to hardware resulted in circuits using on average 117 CNOTs ranging from 108 to 159 CNOTs. As expected, the high frequency signal is well represented in the data, but not the low frequency signal.

VI. CONCLUSION

We demonstrate that for two-site DMFT running on modern quantum hardware, Cartan decomposition is at least as viable as Trotter based simulation in extracting low frequencies from Green's function. However, we have not yet demonstrated convergence of the DMFT loop except for coincidental convergence to $V = 0$ in the Mott insulating phase $U > 6t^*$[8] due to the low amplitudes of the spectral function peaks.

Future work on this project aims to address both issues with the specific circuit implementation and DMFT convergence. Optimal transpiling of the Cartan based circuit onto hardware with only nearest-neighbor qubit connectivity remains challenging due to the cost of SWAP gates in nonlocal Pauli string terms. In the case of Cartan decomposition, these nonlocal Pauli string terms are generated by the $\mathfrak{k}$ decompositon and are not present in the local interaction terms of the Hamiltonian. A possible approach to reducing the circuit complexity is through diagonalization methods allowing simultaneous exponentials of commuting Pauli strings.[12]

For DMFT convergence, we aim to address the frequency analysis by increasing the time domain of the Green's function measurements; normalizing the spectral peaks using spectral function sum rule; and computing the updated V via the derivative of the self-energy. This final step is particularly valuable for the case of overlapping spectral peaks, and would be the first demonstration of solving the two-site DMFT problem on quantum hardware.[1]

ACKNOWLEDGMENTS

The authors would like to thank Eugene F. Dumitrescu, Alexander F. Kemper, Efekan Kökcü, and Trevor Keen for helpful discussion about and feedback on this work. This work was supported in part by the U.S. Department of Energy, Office of Science, Office of Workforce Development for Teachers and Scientists (WDTS) under the Science Undergraduate Laboratory Internship program. Access to the IBM Q Network was obtained through the IBM Q Hub at NC State. We acknowledge the use of the QISKIT software package for performing the quantum simulations.

Appendix: Green's function evaluation

The retarded Green's function is given by

$$G^{\mathrm{R}}_{\mathrm{imp}}(t) = \theta(t)[G^{>}(t) - G^{<}(t)],$$

where the lesser $G^{<}(t)$ and greater $G^{>}(t)$ Green's functions are

$$G^{<}(t) = i\left\langle \psi_{\mathrm{GS}} \middle| \hat{c}_0^{\dagger}\hat{c}_0(t) \middle| \psi_{\mathrm{GS}} \right\rangle,$$
$$G^{>}(t) = -i\left\langle \psi_{\mathrm{GS}} \middle| \hat{c}_0(t)\hat{c}_0^{\dagger} \middle| \psi_{\mathrm{GS}} \right\rangle.$$

Here, $\hat{c}_0(t) = e^{i\hat{H}t}\hat{c}_0 e^{-i\hat{H}t}$ and $\hat{c}_0^{\dagger}(t) = e^{i\hat{H}t}\hat{c}_0^{\dagger}e^{-i\hat{H}t}$.

Denote $U(t) = e^{-i\hat{H}t}$ and apply the Jordan-Wigner transform to these terms, we have

$$\begin{aligned}
G^<(t) &= i\left\langle \psi_{\mathrm{GS}} \middle| \frac{1}{2}(X_0 - iY_0)U^\dagger(t)\frac{1}{2}(X_0 + iY_0)U(t) \middle| \psi_{\mathrm{GS}} \right\rangle \\
&= \frac{i}{4}\left[\left\langle X_0U^\dagger(t)X_0U(t)\right\rangle + i\left\langle X_0U^\dagger(t)Y_0U(t)\right\rangle - i\left\langle Y_0U^\dagger(t)X_0U(t)\right\rangle + \left\langle Y_0U^\dagger(t)Y_0U(t)\right\rangle\right] \\
G^>(t) &= -i\left\langle \psi_{\mathrm{GS}} \middle| U^\dagger(t)\frac{1}{2}(X_0 + iY_0)U(t)\frac{1}{2}(X_0 - iY_0) \middle| \psi_{\mathrm{GS}} \right\rangle \\
&= \frac{-i}{4}\left[\left\langle U^\dagger(t)X_0U(t)X_0\right\rangle + i\left\langle U^\dagger(t)Y_0U(t)X_0\right\rangle - i\left\langle U^\dagger(t)X_0U(t)Y_0\right\rangle + \left\langle U^\dagger(t)Y_0U(t)Y_0\right\rangle\right].
\end{aligned}$$

Measuring the 8 terms in function $4iG^R_{\mathrm{imp}}(t>0) = 4i[G^>(t) - G^<(t)] = \langle X_0(t)X_0\rangle + i\langle Y_0(t)X_0\rangle - i\langle X_0(t)Y_0\rangle + \langle Y_0(t)Y_0\rangle + \langle X_0X_0(t)\rangle + i\langle X_0Y_0(t)\rangle - i\langle Y_0X_0(t)\rangle + \langle Y_0Y_0(t)\rangle$ would require 16 total circuits: two circuits per term for the real and imaginary components, respectively. We reduce the evaluation to only two measurement circuits for real component of the two terms $\langle X_0(t)X_0\rangle$ and $\langle Y_0(t)Y_0\rangle$. The simplification follows

$$\begin{aligned}
&4iG^{\mathrm{R}}_{\mathrm{imp}}(t>0) \\
=&4i[G^>(t) - G^<(t)] \\
=&[\langle X_0(t)X_0\rangle + \langle X_0X_0(t)\rangle] &&+ i[\langle Y_0(t)X_0\rangle + \langle X_0Y_0(t)\rangle] &&- i[\langle X_0(t)Y_0\rangle + \langle Y_0X_0(t)\rangle] &&+ [\langle Y_0(t)Y_0\rangle + \langle Y_0Y_0(t)\rangle] \\
=&[\langle X_0(t)X_0\rangle + \langle X_0(t)X_0\rangle^*] &&+ i[\langle Y_0(t)X_0\rangle + \langle Y_0(t)X_0\rangle^*] &&- i[\langle X_0(t)Y_0\rangle + \langle X_0(t)Y_0\rangle^*] &&+ [\langle Y_0(t)Y_0\rangle + \langle Y_0(t)Y_0\rangle^*] \\
=&2\,\mathrm{Re}\,\langle X_0(t)X_0\rangle &&+ 2i\,\mathrm{Re}\,\langle Y_0(t)X_0\rangle &&- 2i\,\mathrm{Re}\,\langle X_0(t)Y_0\rangle &&+ 2\,\mathrm{Re}\,\langle Y_0(t)Y_0\rangle\,.
\end{aligned}$$

Since at half-filling, due to particle-hole symmetry, the imaginary component of $iG^R_{\mathrm{imp}}(t)$ is zero, we only need to measure the first and last term in the above: the real components $\mathrm{Re}\,\langle X_0(t)X_0\rangle$ and $\mathrm{Re}\,\langle Y_0(t)Y_0\rangle$.

[1] T. Keen, T. Maier, S. Johnston, and P. Lougovski, "Quantum-classical simulation of two-site dynamical mean-field theory on noisy quantum hardware," Quantum Science and Technology **5**, 035001 (2020).

[2] E. Kökcü, T. Steckmann, J. K. Freericks, E. F. Dumitrescu, and A. F. Kemper, "Fixed depth Hamiltonian simulation via Cartan decomposition," arXiv:2104.00728 [cond-mat, physics:quant-ph] (2021).

[3] J. Hubbard, "Electron correlations in narrow energy bands," Proceedings of the Royal Society of London. Series A. Mathematical and Physical Sciences **276**, 238–257 (1963).

[4] G. Kotliar and D. Vollhardt, "Strongly correlated materials: Insights from dynamical mean-field theory," Physics Today **57**, 53–59 (2004).

[5] M. A. Nielsen, "The fermionic canonical commutation relations and the Jordan-Wigner transform," (2005), unpublished.

[6] M. Potthoff, "Two-site dynamical mean-field theory," Physical Review B **64**, 165114 (2001).

[7] J. M. Kreula, L. García-Álvarez, L. Lamata, S. R. Clark, E. Solano, and D. Jaksch, "Few-qubit quantum-classical simulation of strongly correlated lattice fermions," EPJ Quantum Technology **3**, 1–19 (2016).

[8] E. Lange, "Renormalized vs unrenormalized perturbation-theoretical approaches to the Mott transition," Modern Physics Letters B **12**, 915–919 (1998).

[9] H. N. S. Earp and J. K. Pachos, "A constructive algorithm for the Cartan decomposition of $SU(2^N)$," Journal of Mathematical Physics **46**, 082108 (2005).

[10] T. Steckmann and E. Kökcü, (2021), `Cartan Quantum Synthesizer`: https://github.com/kemperlab/cartan-quantum-synthesizer.

[11] M. S. ANIS *et al.*, "Qiskit: An open-source framework for quantum computing," (2021).

[12] P. Gokhale, O. Angiuli, Y. Ding, K. Gui, T. Tomesh, M. Suchara, M. Martonosi, and F. T. Chong, "$O(N^3)$ measurement cost for variational quantum eigensolver on molecular Hamiltonians," IEEE Transactions on Quantum Engineering **1**, 1–24 (2020).